Acta Biochim Biophys Sin 2026, 58(6): 1291–1302
https://cstr.cn/32197.14.abbs.2026036
https://doi.org/10.3724/abbs.2026036
Original Article

Original Article

Structural basis for the FOXM1 DNA binding domain to specific dsDNA substrate

Mingxuan Sun[1], Lei Wang[1], Jing Cui[1], Liang Zhang[1], Yunyu Shi[1], Chao Xu[1,*], Wanwan Zhou[1,*], and Mengqi Lv[2,*]

[1]Hefei National Research Center for Cross disciplinary Science, School of Life Sciences, Division of Life Sciences and Medicine, University of Science and Technology of China, Hefei 230027, China, and [2]Department of Hepatobiliary Surgery, Innovative Institute of Tumor Immunity and Medicine (ITIM), Anhui Province Key Laboratory of Tumor Immune Microenvironment and Immunotherapy, the First Affiliated Hospital of Anhui Medical University, Hefei 230022, China

*Correspondence address. E-mail: xuchaor@ustc.edu.cn (X.C.); zhouww@ustc.edu.cn (W.Z.); lmq123@ustc.edu.cn (M.L.)

Received 12 December 2025 Accepted 2 March 2026 Published 27 March 2026

Abstract

Forkhead box protein M1 (FOXM1) is a key transcription factor that regulates cell cycle progression and is frequently overexpressed in human cancers, driving tumor proliferation and therapy resistance. FOXM1 recognizes the canonical forkhead response element (FKH motif, RYAAAYA) through its conserved DNA-binding domain (DBD). Here, we report the high-resolution crystal structure of the FOXM1-DBD in complex with a double-stranded DNA substrate containing two FKH motifs. The structure reveals that FOXM1-DBD adopts the canonical winged-helix fold, with the third α-helix (α3) inserted into the DNA major groove to mediate sequence-specific recognition. Within this helix, Asn283, Arg286, and His287 form an essential triad that engages DNA bases through specific hydrogen bonds and hydrophobic interactions. Using structure-guided mutagenesis of key DNA-interacting residues combined with biophysical validation by isothermal titration calorimetry (ITC) and DNA binding assessment via electrophoretic mobility shift assay (EMSA), we confirm the functional importance of these residues and uncover position-dependent tolerance to base substitutions within the FKH motif. Furthermore, we demonstrate that FOXM1 overexpression promotes cell proliferation and upregulates the transcription of target genes in a DBD-dependent manner. Our findings provide a structural basis for understanding the DNA recognition mechanism of FOXM1 and offer mechanistic insights into how FOXM1 selectively binds to its genomic targets to regulate transcription.

Key words transcription factor, FOXM1, DNA-binding domain, protein-dsDNA binding, crystal structure

Introduction

The precise regulation of cell cycle progression is fundamental to cellular homeostasis, and its dysregulation underlies the pathogenesis of numerous human diseases [1,2]. In eukaryotes, this process is governed by an integrated network of cyclins, cyclin-dependent kinases (CDKs), checkpoint signaling pathways, and ubiquitin-mediated regulatory mechanisms [3,4]. When this sophisticated control system is compromised, it contributes not only to cancer development but also to a spectrum of other pathological conditions, including cardiovascular disorders, inflammatory diseases, and neurodegenerative processes [2]. Understanding the molecular mechanisms that maintain cell cycle-metabolic coordination is therefore essential for elucidating fundamental biological processes such as differentiation and aging while also providing critical insights for addressing disease mechanisms.

Within this regulatory framework, transcription factors (TFs) serve as crucial intermediaries that translate cell cycle signals into specific gene expression programs [5,6]. As sequence-specific DNA-binding proteins, TFs recognize distinct regulatory elements to establish phase-dependent gene expression patterns essential for orderly cell cycle progression [7,8]. This regulatory system features intricate feedback mechanisms, as many TFs themselves exhibit cell cycle-dependent expression or activity, creating sophisticated regulatory circuits with CDK/cyclin complexes [9,10]. Through these reciprocal interactions, TFs coordinate the sequential activation of genes governing critical cell cycle transitions while

© The Author(s) 2026. This is an open access article distributed under the terms of the Creative Commons Attribution-NonCommercial-NoDerivs License (https://creativecommons.org/licenses/by-nc-nd/4.0/).

simultaneously integrating extracellular signals to ensure that division occurs only under appropriate conditions. The crucial role of TFs in cell cycle control is frequently exploited in cancer pathogenesis [11]. Malignant cells commonly overexpress specific TFs to drive proliferation and increase survival [12]. Notably, many cancers are dependent on lineage-specific TFs that normally regulate cell fate decisions and differentiation programs [5,13]. This appropriation of developmental regulatory mechanisms represents a fundamental strategy by which cancer cells maintain their proliferative advantage and survival capacity.

Among the transcriptional regulators governing cell cycle progression, FOXM1 has emerged as a master regulator that integrates the core cell cycle machinery with transcriptional outputs [14,15]. As a member of the evolutionarily conserved Forkhead box (FOX) superfamily [16–18] comprising 44 human members [19,20], FOXM1 displays precisely orchestrated expression dynamics throughout the cell cycle, with levels initiating their rise in late G1, peaking during S-phase, and remaining elevated through G2/M phases [21]. This temporal expression pattern aligns with its fundamental role in controlling genes essential for cell cycle progression, including key regulators such as CDC20, CDC25 phosphatases, and cyclins A and B [22,23]. The oncogenic potential of FOXM1 is demonstrated by the strong correlation between its aberrant activation and poor clinical outcomes across multiple cancer types [24], while its inhibition has been shown to attenuate chemoresistance, invasion, and migration [16,25]. The mechanistic basis underlying FOXM1 function involves multiple regulatory layers, including liquid-liquid phase separation (LLPS), which facilitates its DNA binding in breast cancer cells [26], cooperative interactions with ASPM, which increases its stability in hepatocellular carcinoma [24], and nuclear association with LC3, which enables the transfer of FOXM1-bound chromatin fragments via exosomes [27]. FOXM1 activity is precisely controlled through posttranslational modifications. Phosphorylation events initiated by CDKs create docking sites for PLK1, which subsequently phosphorylates FOXM1 to relieve autoinhibition [28], whereas upstream regulation involves E2F1-mediated transactivation, particularly in the contexts of compromised p53/Rb pathways [29], and RAF/MEK/ERK signaling, which promotes FOXM1 phosphorylation and nuclear localization [30]. Conversely, FOXM1 is targeted for degradation at mitotic exit via the APC/C-Cdh1 complex [31], completing its cell cycle-coupled regulation. Through these multifaceted regulatory mechanisms, FOXM1 establishes itself as a central coordinator of mitotic progression whose dysregulation profoundly contributes to cancer pathogenesis.

Structurally, all members of the FOX superfamily possess a highly conserved DNA-binding domain known as the forkhead or winged-helix domain [32]. This domain is characterized by a three-helix bundle (α1, α2, α3) followed by two β-strands and variable wing loops (W1, W2). High-resolution structures of several FOX family DNA-binding domains (DBDs)—such as FOXO1, FOXA2, and FOXK1—bound to DNA have revealed a common recognition mode in which the third helix (α3) inserts into the DNA major groove for base-specific readout, while wing regions often engage the phosphate backbone to modulate affinity. Despite this conserved overall fold, significant variations exist across different FOX subfamilies in the precise interaction networks, the conformation and functional role of wing regions, and the resulting DNA-binding affinity and specificity. As a key regulator of proliferation and oncogenesis, FOXM1 represents an ideal subject for structural study to delineate how its DBD engages DNA within this conserved yet adaptable family framework. FOXM1 contains an N-terminal repressor domain, a central DBD that includes the forkhead (FKH) domain and intrinsically disordered regions, and a C-terminal transactivation domain harboring multiple phosphorylation sites [23,26,33]. The protein recognizes and binds to the canonical forkhead response element (RYAAAYA, FKH motif) through its conserved DNA-binding domain [34–36], with recent evidence indicating that its intrinsically disordered regions influence DNA binding through phase separation mechanisms [23]. In addition to its direct DNA recognition capabilities, FOXM1 engages in functional partnerships with diverse protein interactors—including ASPM in hepatocellular carcinoma and SMAD3 in breast cancer—often establishing self-reinforcing positive feedback loops that amplify its oncogenic potential [24,37].

Given the central role of FOXM1 in oncogenesis, structural and biochemical characterization of the complex formed between its DNA-binding domain and the FKH motif represents a crucial step toward a mechanistic understanding of FOXM1-mediated regulation. In this study, we aimed to elucidate the molecular details of FOXM1-DNA interactions by determining the crystal structure of its Forkhead DNA-binding domain in complex with a double-stranded DNA (dsDNA) substrate containing two potential FOXM1 recognition motifs. By integrating crystallographic approaches with biophysical and biochemical validation methods, we seek to delineate the precise molecular determinants of binding specificity and establish the structural basis for genomic targeting of FOXM1. These insights will provide a foundation for understanding how FOXM1 establishes its oncogenic transcriptional programs and will inform future therapeutic strategies aimed at disrupting these pathways in cancer.

Materials and Methods

Cloning, protein expression, and purification

A DNA fragment encoding the DNA-binding domain (residues 222–360) of human *FOXM1* was amplified via PCR from a human brain cDNA library and cloned and inserted into a modified pGEX-4T-1 vector (Novagen, Darmstadt, Germany), in which the thrombin cleavage site was replaced by a tobacco etch virus (TEV) protease site. All FOXM1 mutants were generated using the MutanBEST kit (TaKaRa, Kusatsu, Japan) and verified via DNA sequencing. As previously described [38], protein expression was carried out in *Escherichia coli* Rosetta (DE3) cells (Novagen). The bacteria were grown in LB medium at 37°C until an OD_{600} of approximately 0.9 was reached, then transferred to 16°C and induced with 0.2 mM isopropyl-β-D-thiogalactopyranoside (IPTG) overnight. The cells were harvested via centrifugation, resuspended in buffer A (50 mM Na_2HPO_4 and 500 mM NaCl, pH 7.0), and lysed via sonication on ice.

The fusion proteins were affinity-purified via glutathione-Sepharose beads (GE Healthcare, Waukesha, USA) in buffer B (50 mM Na_2HPO_4 and 350 mM NaCl, pH 7.0). The GST tag was removed by on-column cleavage with TEV protease overnight at 16°C. The protein was further purified by size-exclusion chromatography on a Superdex 200 column (GE Healthcare) and finally dialyzed into buffer C (50 mM Na_2HPO_4 and 150 mM NaCl, pH 7.0) for crystallization.

DNA synthesis and annealing

The single-stranded oligonucleotides were synthesized by General

Biol Co., Ltd. (Hefei, China) and dissolved in buffer C to a final concentration of 1 mM. Equimolar amounts of complementary strands were mixed in a microtube, denatured by heating at 95°C for 5 min, and then gradually cooled on ice for another 5 min to promote annealing. Next, the double-stranded DNA was diluted to the desired concentrations and subsequently used in both crystallization trials, isothermal titration calorimetry (ITC) and electrophoretic mobility shift assay (EMSA). Sequences of all DNA oligonucleotides employed in this study are provided in Supplementary Table S1.

Crystallization

The FOXM1-DBD proteins were directly added to the prepared 24-bp double-stranded oligo with a 5′-overhang at a 1:1.5 molar ratio, followed by separation on the Superdex 200 column in buffer C to remove the excess DNA. The complex was further concentrated up to approximately 2 mM. Crystals of the FOXM1-DBD-dsDNA complex were grown at 16°C using the sitting drop vapor diffusion method, with a mother liquor containing 10% PEG 20000, 0.1 M sodium citrate tribasic dihydrate (pH 5.0) and 0.2 M magnesium chloride hexahydrate.

X-ray diffraction data collection

Crystals were protected in the mother liquor supplemented with 20% glycerol before being flash-frozen in liquid nitrogen. X-ray diffraction data for the crystals were collected on beamline 02U1 of the Shanghai Synchrotron Radiation Facility (SSRF, Shanghai, China). Data were indexed, integrated and scaled with XDS and programs in the CCP4i suite.

Structure determination

For the FOXM1-DBD-dsDNA complex, the structure of the DBD domain was solved via molecular replacement with the program Phaser and MOLREP [39] in the CCP4 program suite, with the AlphaFold model of FOXM1 as the search model (ID: AF-Q08050-F1, residues 222–360). The dsDNAs were then built manually using COOT [40]. All initial models were refined using the maximum likelihood method implemented in REFMAC5 [41,42] as part of the CCP4i program suite and rebuilt interactively using the program COOT. The final refinement strategies included XYZ coordinates, individual B-factors, occupancies, and automated correction of N/Q/H errors using PHENIX [43]. The crystallographic parameters are listed in Table 1. All images of the structures were prepared using PyMOL (http://www.pymol.org/).

Isothermal titration calorimetry

ITC assay was conducted at 20°C using a Microcal PEAQ-ITC instrument (Malvern, Westborough, USA). The concentrations of GST-tagged FOXM1-DBD and its mutant variants were determined by absorbance measurements. Proteins and dsDNA were dialyzed against buffer C and adjusted to 30 μM and 500 μM, respectively. The titration protocol was the same for all the measurements, composed of a single initial injection of 1 μL of dsDNA, followed by 19 injections of 2 μL of dsDNA into protein samples. The intervals between injections were set to 120 s, and the reference power was 5 $\mu cal \cdot s^{-1}$. The thermodynamic data were analyzed with a single binding site model using Microcal PEAQ-ITC analysis software provided by the manufacturer. The thermodynamic parameters of the ITC experiments are listed in Supplementary Table S2.

Table 1. Data collection and refinement statistics

Data collection	FOXM1-DBD-dsDNA complex
Beamline	BL02U1, SSRF
Space group	I_2
PDB code	9XS1
Wavelength (Å)	0.979
Resolution (Å)	38.50–2.50 (2.59–2.50)[a]
Cell dimensions	
a, *b*, *c* (Å)	72.21, 45.61, 213.49
α, *β*, *γ* (°)	90, 95.82, 90
Unique reflections	24027 (2686)
Completeness (%)	98.5 (98.7)
Redundancy	6.6 (7.1)
$I/\sigma I$	10.8 (2.6)
R_{merge} (%)	8.6 (89.1)
$CC^{1/2}$	99.7 (87.4)
Refinement	
R_{work} (%)	21.26
R_{free} (%)	24.86
Numbers of atoms	
Protein	1760
DNA	1956
Water	20
Average B factors (Å^2)	
Protein	78.55
DNA	113.11
Water	65.04
Root mean square deviations	
Bond lengths (Å)	0.010
Bond angles (°)	1.161
Ramachandran plot	
Favored (%)	94.61
Allowed (%)	5.39
Disallowed	0

[a]Values for the highest-resolution shell are shown in parentheses.

Electrophoretic mobility shift assay

All DNA-binding reactions were carried out in binding buffer C. EMSA was performed using DNA substrates that were not chemically labeled. Before use, the DNA substrates were heat denatured at 95°C for 5 min and subsequently annealed on ice for 5 min. A total of 10 μL of each binding reaction assay consisted of 5 μL of 0.8 μM DNA substrate and 5 μL of GST-tagged FOXM1-DBD at varying concentrations. FOXM1-DBD was initially diluted to 80 μM and then further diluted in successive 2-fold increments to achieve a final concentration of 0.4 μM. Reactions were then generated by incubation at room temperature for 15 min and analysis via 6% native polyacrylamide gels using 0.5× TBE (44.5 mM Tris, 44.5 mM H_3BO_3, and 1.0 mM EDTA) as running buffer at 120 V for 35 min. The gels were stained with GelRed (PP508; Protein Biotechnologies, Beijing, China) for visualization and scanned using GenoSens 2000 (Clinx Corp., Shanghai, China), unless otherwise specified.

Cell culture and cell proliferation assay

HepG2 cells (QC163; Qincheng Biotechnology, Shanghai, China) were cultured in Dulbecco's modified Eagle's medium (DMEM; 11995065; Gibco, Carlsbad, USA) supplemented with 10% fetal bovine serum (FBS; FSP500; ExCell, Shanghai, China) at 37°C in a 5% CO_2 atmosphere. To investigate the role of FOXM1 in cell proliferation, the cells were transfected with the following C-terminally Flag-tagged constructs: a full-length wild-type FOXM1 ($FOXM1_{FL}$-Flag), a DNA-binding domain deletion mutant ($FOXM1_{FL}$-ΔDBD-Flag), and a series of DBD point mutants ($FOXM1_{FL}$-mut-Flag). At 24 h post-transfection, cells were seeded into a 96-well plate at a density of 2000 cells per well ($n = 6$ per group). Cell proliferation was assessed every 24 h using the CCK-8 assay kit (BMU106; Abbkine Scientific Co., Ltd., Wuhan, China). Briefly, 10 μL of CCK-8 solution was added to each well containing 100 μL of culture medium, followed by incubation for 3.5 h at 37°C. The absorbance at 450 nm was then measured to generate a kinetic proliferation profile.

Real-time quantitative PCR

HepG2 cells were transfected with the aforementioned FOXM1 plasmids (including wild-type and mutant variants) for 48 h. Total RNA was then extracted from the transfected cells and reverse-transcribed into cDNA using a standard protocol. The expression levels of target genes were analyzed by qPCR with gene-specific primers. Transcript levels were normalized to the housekeeping gene *GAPDH*. The sequences of all primers are provided in Supplementary Table S1.

Western blot analysis

HepG2 cells were collected for western blot analysis. Cell lysates were prepared in RIPA buffer (50 mM Tris-HCl, pH 8.0, 150 mM NaCl, 5 mM EDTA, 0.1% SDS, and 1% NP-40) supplemented with a protease inhibitor cocktail (Roche, Basel, Switzerland). Equal amounts of total cell lysates were separated by SDS-PAGE. The following primary antibodies were used: anti-Flag (20543-1-AP; Proteintech, Wuhan, China) and anti-GAPDH (HRP-60004; Proteintech; using as a loading control). Horseradish peroxidase-conjugated anti-rabbit secondary antibody (STAR121; Bio-Rad, Hercules, USA) was used to detect primary antibody binding, and the signal was detected using a LAS4000 mini (GE Healthcare).

Statistical analysis

Statistical analysis was performed using Origin software. All experiments were independently repeated at least three times, and data are presented as the mean ± standard deviation (SD). Comparisons among multiple groups were conducted using one-way ANOVA with Tukey's post hoc test, and $P < 0.05$ was considered statistically significant.

Results

Micromolar-affinity binding of FOXM1-DBD to specific dsDNA substrates

To characterize the DNA-binding ability of the FOXM1 DNA-binding domain (FOXM1-DBD, residues 222–360) to specific dsDNA substrate, we designed a dsDNA substrate containing two potential FOXM1-binding motifs (Figure 1A). This sequence represents the high-affinity FOXM1 recognition element previously identified by SELEX [44]. The tandem arrangement was chosen to promote stable complex formation for crystallization while preserving the biologically relevant, consensus binding sequence. Recombinant FOXM1-DBD was expressed in an *E. coli* expression system and purified to homogeneity (Figure 1B,C). EMSA confirmed a strong interaction between FOXM1-DBD and the dsDNA substrate (Figure 1D). ITC assay further quantified the binding affinity, yielding a dissociation constant (K_d) of 1.86 ± 0.20 μM (Figure 1E). The binding stoichiometry ($N \approx 0.5$) derived from ITC is consistent with two FOXM1-DBD molecules binding independently, each to one of the two ATAAACA motifs within the dsDNA substrate, in a non-cooperative manner.

Overall structure of the FOXM1-DBD-dsDNA complex

To elucidate the structural basis of FOXM1-specific dsDNA substrate recognition, we tried to crystallize the complex formed by FOXM1-DBD and the 24 bp dsDNA substrate. After extensive efforts, we successfully obtained well-diffracted crystals. Crystals were grown at 16°C via the hanging drop vapor diffusion method, with the mother liquor. The crystal structure of the FOXM1-DBD-dsDNA complex was determined in space group I2 and refined to a resolution of 2.5 Å. The crystal structure was solved by molecular replacement using the AlphaFold model of FOXM1 (ID: AF-Q08050-F1, residues 222–360) as the search model. Finally, the R_{work} and R_{free} values of the FOXM1-DBD-dsDNA complex structure were refined to 21.26% and 24.86%, respectively. The detailed crystallographic statistics are summarized in Table 1.

The crystallographic asymmetric unit contained two FOXM1-DBD-dsDNA complexes (Figure 2A). Although the dsDNA substrate bears two tandem FOXM1-binding motifs, which would suggest a 2:1 protein-to-DNA stoichiometry, the complexes within the asymmetric unit exhibited a mixed composition: one comprised a 2:1 FOXM1-DBD-dsDNA complex, whereas the other was a 1:1 complex. This deviation from the expected stoichiometry may arise from crystal packing constraints that stabilize this particular arrangement for optimal lattice formation. The presence of both complexes in the crystal should therefore be regarded as a packing artifact, not as representative of the binding behavior in solution. Consistently, the ITC data indicate that the two FOXM1-DBD molecules bind independently to the tandem sites in solution. Aside from the absence of one DBD bound to the second ATAAACA motif in the 1:1 complex, the overall conformations of the two complexes were highly similar, with a root-mean-square deviation (RMSD) of 0.21 Å over 69 aligned Cα atoms of the FOXM1-DBD (Figure 2B). Given their structural similarity, we focused subsequent analysis on the 2:1 FOXM1-DBD-dsDNA complex.

Analysis of the 2:1 FOXM1-DBD-dsDNA complex revealed continuous electron density for the entire DNA and the first FOXM1-DBD (FOXM1-DBD1, residues 236–312) (Supplementary Figure S1). The map for the second FOXM1-DBD (FOXM1-DBD2, residues 237–311) was of lower quality. Specifically, poor density for segments 274–278 and 298–307 precluded their model building (Supplementary Figure S2). Additionally, no interpretable electron density was observed for the N- and C-terminal regions in either FOXM1-DBD molecule, indicating structural flexibility or disorder in these terminal segments.

Similar to other FOX family proteins, the FOXM1-DBD in our complex structure adopts the canonical Forkhead box winged-helix

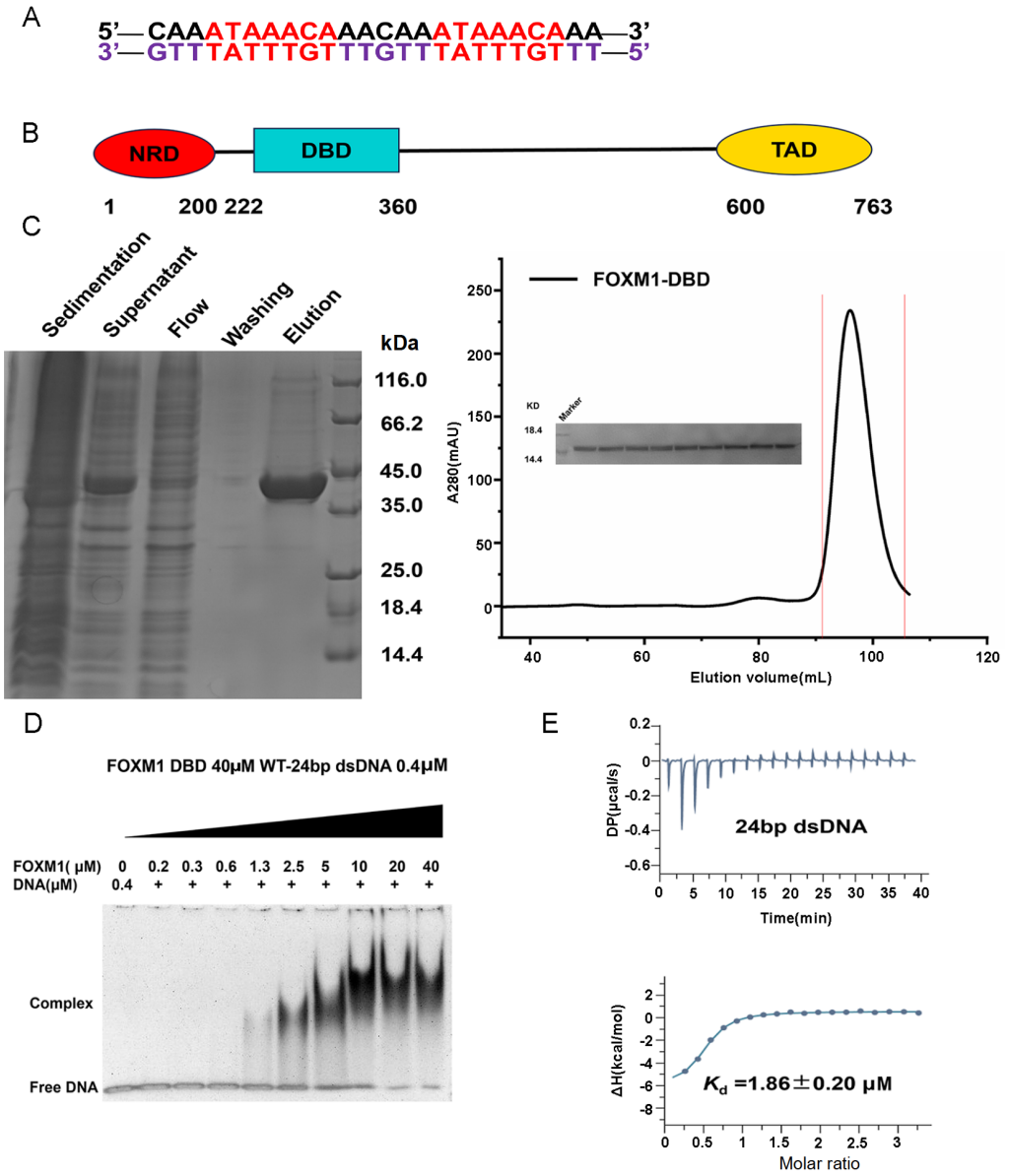


Figure 1. Characterization of the FOXM1 DNA-binding domain (A) Schematic of double-stranded DNA (dsDNA) containing two FOXM1 binding motifs (highlighted in red). The motif sequences were identified by SELEX and are reproduced from Ref [44]. (B) The domain architecture of the FOXM1 transcription factor is shown. (C) Purification and oligomeric state of the FOXM1-DBD. The gel filtration profile indicated a monomeric state, and SDS-PAGE analysis confirmed the purity of FOXM1-DBD. (D) EMSAs were performed with dsDNA and increasing concentrations of FOXM1-DBD. (E) ITC binding isotherm and fitted curve for FOXM1-DBD titrated with 24 bp dsDNA. DP, differential power; ΔH, enthalpy change; n = 3 replicates.

fold (Figure 3A). The conserved architecture consists of a bundle of three α-helices (α1, α2, α3), followed by a β-hairpin composed of two anti-parallel β-strands (β1, β2) and a characteristic flexible wing loop (W1). The overall topology follows the sequential order from the N- to C-terminus: α1-α2-α3-β1-W1-β2. FOXM1-DBD engages the specific dsDNA substrate primarily through its third helix (α3), which presents a positively charged surface that inserts into the major groove of DNA. The two FOXM1-DBD domains mediate sequence-specific recognition by contacting the tandem 7-bp ATAAACA consensus FKH motifs in the specific dsDNA substrate (Figure 3A and Supplementary Table S3). To facilitate a clear description of the protein-DNA interactions, the DNA sequence is numbered with the first nucleotide of the first consensus motif as position 0 (site: ^{0}ATAAACA^{6}) and the first nucleotide of the second motif as position 12 (site: ^{12}ATAAACA^{18}) (Figure 3B).

Molecular basis of DNA recognition by FOXM1-DBD

FOXM1-DBD engages its target DNA through a combination of sequence-specific and non-sequence-specific interactions, as summarized in Figure 3A and Supplementary Table S3. Helix α3 from the first FOXM1-DBD molecule (FOXM1-DBD1) inserts deeply into the major groove, enabling specific recognition of the first FKH motif. In parallel, helix α3 from the second molecule (FOXM1-DBD2) binds to the adjacent major groove, facilitating interaction

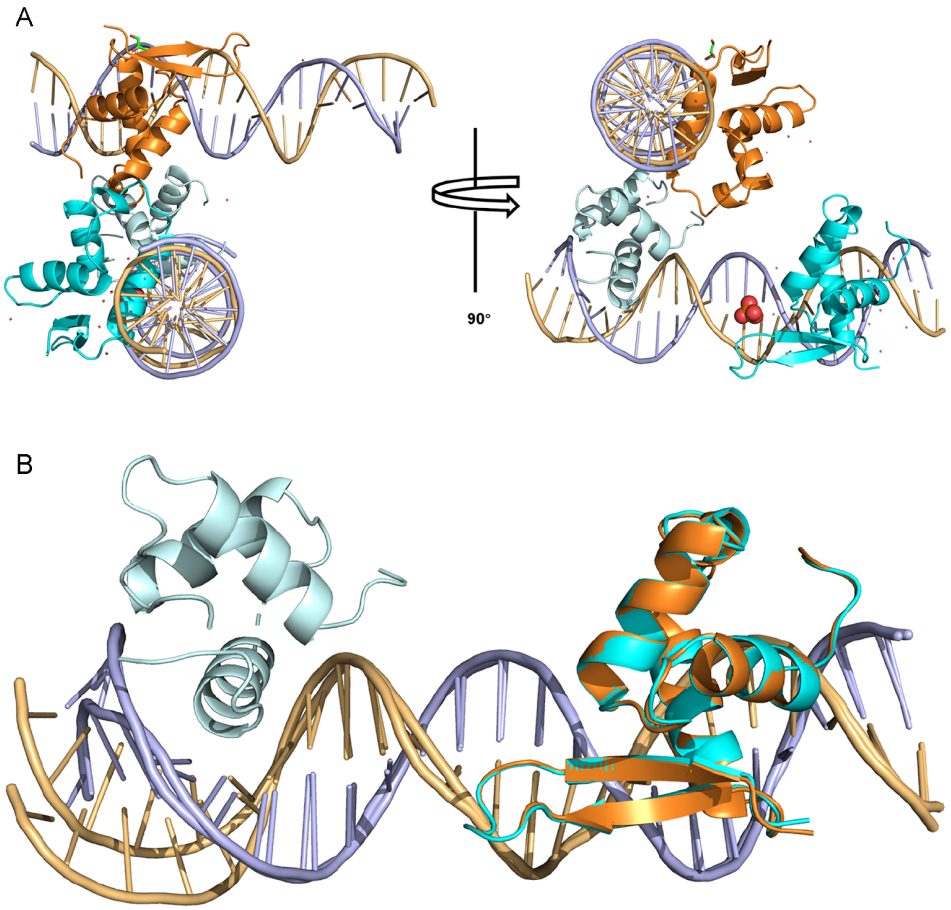


Figure 2. Crystal structure of the FOXM1 DNA-binding domain in complex with dsDNA (A) Overall view of the FOXM1-DBD-dsDNA complex along the DNA axis: top view (left) and side view (right). 2:1_FOXM1-DBD1 is colored cyan, 2:1_FOXM1-DBD2 pale cyan, and 1:1_FOXM1-DBD1 light orange. The dsDNA is shown in light orange and light blue. Structures represent two independently determined complexes. (B) Structural superposition of the 2:1 and 1:1 FOXM1-DBD-dsDNA complexes.

with the second FKH motif (Figure 3A).

For FOXM1-DBD1, non-sequence-specific contacts are mediated primarily by three regions interacting with the DNA backbone: the N-terminal loop preceding helix α1, the N-terminus of helix α2, and residues in β-strands β1 and β2 (Figure 3A). Specifically, the side chains of Arg236 and Tyr241, along with the main chain of Tyr241 in the N-terminal loop, contact the phosphate backbone of one DNA strand. On the opposite strand, the side chains of Leu259 and Lys260 (the N-terminus of α2), as well as Ser290 (α3), Arg297 (β1), Ser306, and Trp308 (β2), engage the phosphate backbone. These interactions collectively span the entire major groove, allowing FOXM1-DBD1 to precisely accommodate and recognize the specific width of the DNA major groove (Figure 3A).

The sequence-specific recognition of the first FKH motif by FOXM1-DBD1 is mediated primarily by key residues located within helix α3. These include the highly conserved residues Asn283, Ser284, Arg286, His287, and Leu291 (Supplementary Figure S3), which collectively interact with DNA bases spanning from T:A1 to C:G5 of the dsDNA. A detailed analysis reveals that Asn283 forms direct bidentate hydrogen bonds with the A3 purine ring: its side-chain amide group donates a hydrogen bond to the N7 atom of adenine while simultaneously accepting a hydrogen bond from the N6 amino group of the same base (Figure 3C). Additionally, the Nε atom of the Arg286 side chain donates a hydrogen bond to the N7 atom of the guanine base at position G5 (Figure 3C). His287 plays a dual role in base recognition: its Nε2 atom donates a hydrogen bond to the O4 carbonyl oxygen of T1, while its Nδ1 atom forms a similar hydrogen bond with the O4 atom of T2 (Figure 3C). Furthermore, the side chains of Ser284 and Leu291 engage in hydrophobic interactions with the methyl groups of T1 and T2, respectively, thereby enhancing the stability and specificity of the protein-DNA interface (Figure 3C).

Structural alignment of FOXM1-DBD1 and FOXM1-DBD2 reveals a high degree of similarity, with a Cα RMSD of 0.314 Å for 53 equivalent residues. Consequently, despite the poorly defined density for some side chains in FOXM1-DBD2, its DNA-binding mode, particularly the key interactions made by helix α3, is conserved relative to that of FOXM1-DBD1 (Supplementary Figure S4).

In summary, structural analysis reveals that sequence recognition is mediated primarily by conserved residues in helix α3, which are inserted into the major groove to form specific hydrogen bonds and hydrophobic contacts with the FKH motif. Additionally, extensive interactions between multiple protein regions and the DNA backbone stabilize the complex and precisely accommodate the geometry of the major groove.

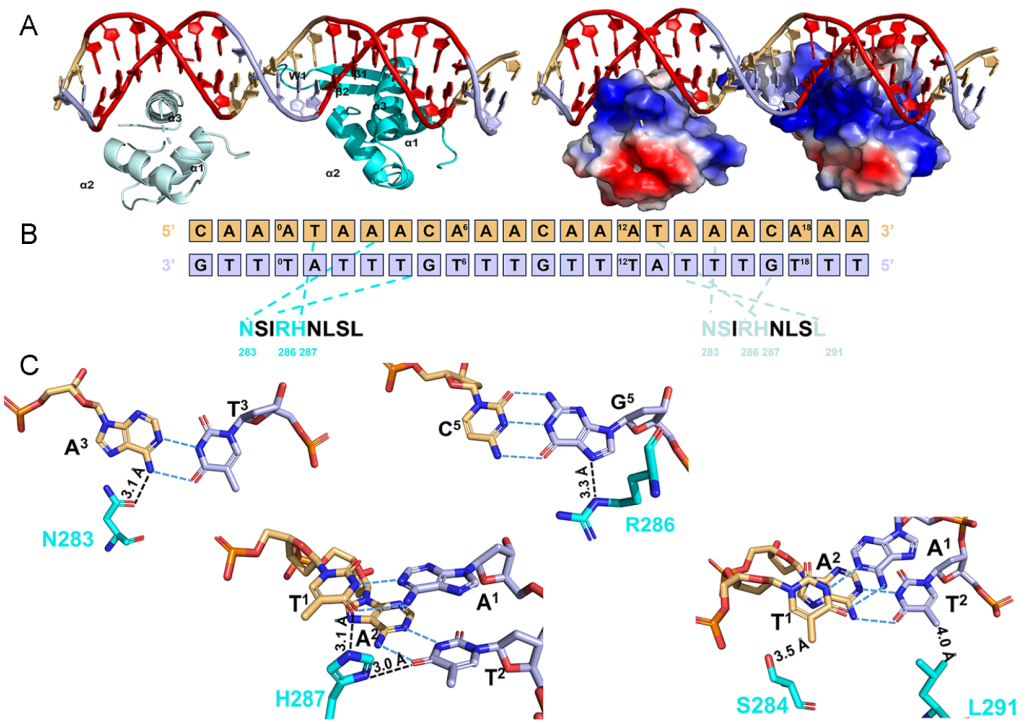


Figure 3. Molecular interactions in the FOXM1-DBD-dsDNA complex (A) Left: structure of the FOXM1 homeobox domain bound to dsDNA via helix α3, with secondary structure elements labeled. Right: electrostatic surface potential of FOXM1-DBD is shown, in which positively charged, negatively charged, and neutral areas are represented in blue, red, and white, respectively. (B) Schematic representation of the interactions between dsDNA and the FOXM1-DBD. Hydrogen bonds are indicated by dotted lines. To facilitate a clear description of the protein-DNA interactions, the DNA sequence is numbered with the first nucleotide of the first consensus motif designated as position 0 and that of the second motif as position 12. (C) Higher magnification views of base-specific contacts between FOXM1-DBD (labeled cyan) and dsDNA (labeled black). Hydrogen bonds are indicated with dotted lines, with distances measured in Å. Black dashed lines represent hydrogen bonds between protein and DNA; cornflower blue dashed lines indicate base-pair hydrogen bonds. All structural images were prepared using PyMOL.

Effects of structure-based mutations in FOXM1-DBD and DNA on the binding affinity *in vitro*

Sequence alignment indicates that key DNA-binding residues in FOXM1-DBD, especially those clustered in helix α3, are highly conserved across the FOX protein superfamily (Supplementary Figure S3). To determine whether these key residues of the FOXM1-DBD are required for binding to the substrate dsDNA *in vitro*, we introduced alanine substitutions into FOXM1-DBD and evaluated their impact on dsDNA binding via ITC and EMSA.

Mutational analysis revealed that residues involved in phosphate backbone contacts contribute differently to DNA binding. Compared with wild-type FOXM1-DBD, single alanine substitutions at Arg236, Tyr241, Ser290, or Trp308 nearly abolished binding, while K260A and R297A reduced binding affinity by approximately 3 folds (K_d = 3.76 ± 0.63 μM) and 2 folds (K_d = 2.48 ± 1.12 μM), respectively. Moreover, as expected, alanine substitution of residues in helix α3, which mediates major groove recognition, significantly impaired the DNA binding of the FOXM1-DBD with the dsDNA substrate (Supplementary Table S2). The single-point mutations N283A, R286A, and H287A essentially abolished the binding activity of FOXM1-DBD (Figure 4A,B), whereas the S284A and L291A mutations exhibited binding affinities comparable to the wild type (Figure 4A,B). These results demonstrate that Asn283, Arg286, and His287 constitute an essential triad within helix α3 that is responsible for sequence-specific recognition in the major groove of DNA.

To systematically delineate the contribution of core bases (T:A1 to C:G5) to binding specificity, we performed a comprehensive mutagenesis scan by introducing single-nucleotide substitutions across this region in the wild-type dsDNA. The binding affinity of FOXM1-DBD for each mutant oligonucleotide was quantified by ITC to evaluate its tolerance to base-pair changes (Supplementary Table S2).

Detailed analysis revealed markedly different effects depending on the specific base substitution. At position T:A1, substitution with G:C (T1G) significantly reduces the binding affinity (K_d = 3.08 ± 0.99 μM), whereas replacement by C:G (T1C) results in substantially weaker binding that approaches the detection limit of ITC (Figure 4A). The critical importance of this position is structurally explained by its dual recognition by both His287 and Ser284, which collectively enforce strict sequence specificity. Position A:T2 demonstrates a remarkable discrimination pattern, where replacement by C:G (A2C) caused an approximately 2.5-fold reduction in binding affinity (K_d = 3.49 ± 0.98 μM), whereas substitution with G:C (A2G) severely diminished binding (Figure 4A). This striking contrast between the two purine substitutions indicates recognition mechanisms that extend beyond simple base classification, with structural analysis revealing that A:T2 is jointly recognized by His287 and Leu291, enabling precise molecular discrimination. The specificity profile at position A:T3 further confirms this pattern of exacting base requirements. Replacement by C:G (A3C) remains measurable although reduced binding (K_d = 3.25 ± 0.98 μM), whereas substitution with G:C (A3G) eliminates detectable binding (Figure 4A). This complete loss of affinity with A3G is resulted from

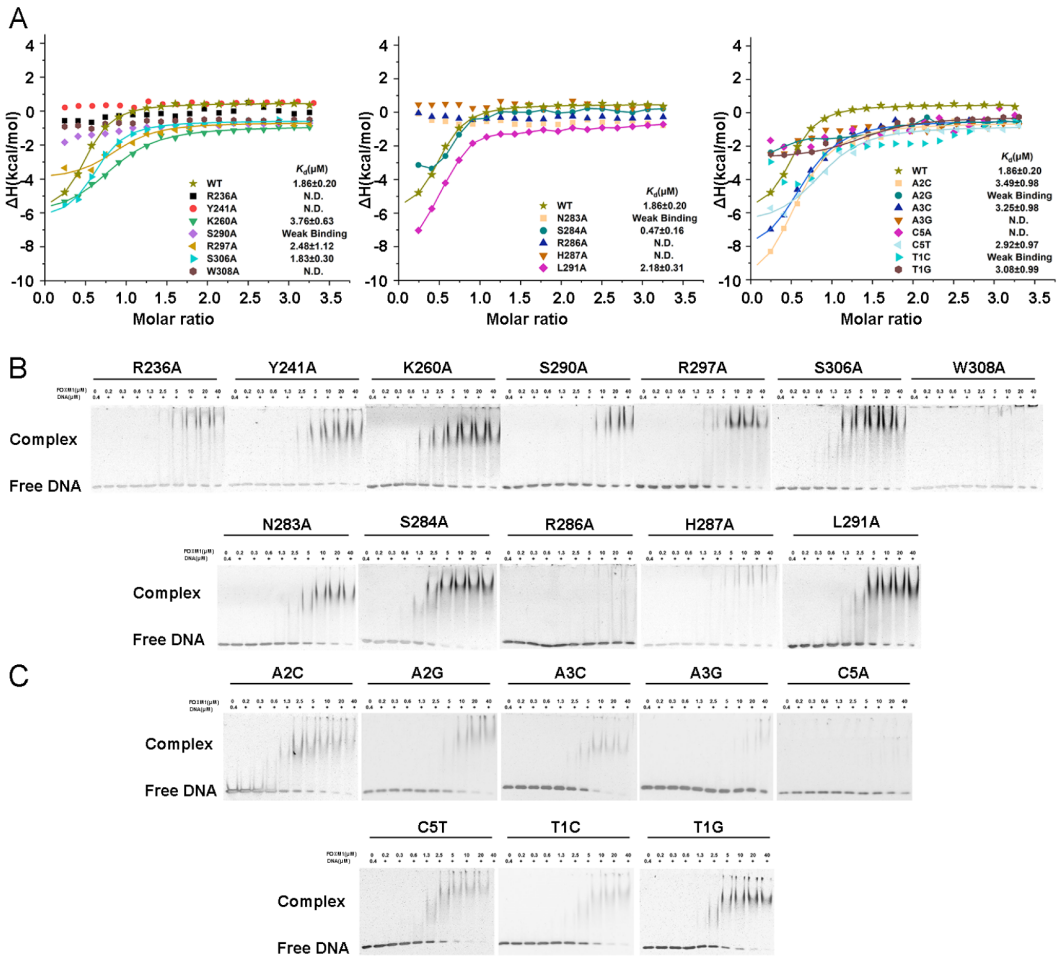


Figure 4. Mutational analysis of FOXM1-dsDNA binding (A) ITC-derived binding affinities (K_d) of FOXM1-DBD for wild-type and mutant dsDNA, including key DNA-binding residues, phosphate-backbone contact residues, and specific base substitutions. Each K_d value is presented as a fitted value ± SD. N.D., no detectable binding. (B) EMSA analysis of dsDNA binding by wild-type and mutant FOXM1-DBD proteins at increasing concentrations. Mutations in key DNA-binding and backbone-contact residues impair DNA-protein complex formation compared to the wild-type protein. (C) EMSA analysis of wild-type FOXM1-DBD binding to key dsDNA variants. Increasing protein concentrations were used to titrate each dsDNA substrate. Mutations at critical base pairs impair DNA-protein complex formation relative to the wild-type dsDNA control.

disruption of essential hydrogen bond interactions with Asn283. Similarly, position C:G5 exhibits pronounced discrimination, with replacement by T:A (C5T) maintaining substantial binding (K_d = 2.92 ± 0.97 μM), whereas substitution with A:T (C5A) severely compromised the interaction (Figure 4A). The detrimental effect of C5A substitution stems from the disruption of key hydrogen bonds with the Arg286 side chain. Correspondingly, EMSAs with key DNA variants confirmed these affinity trends (Figure 4C).

Collectively, these findings demonstrate that FOXM1-DBD recognizes its DNA target through a sophisticated mechanism exhibiting distinct position-dependent specificity and differential tolerance to base substitutions. Each position within the core motif displays unique sensitivity to specific base changes, reflecting the precise structural requirements for optimal binding.

FOXM1 overexpression promotes HepG2 cell proliferation and upregulates the transcription of target genes

As a key proliferation-associated transcription factor, FOXM1 regulates the expression of multiple cell cycle-related genes, coordinating critical processes in DNA replication and mitosis [22,23,34,45–48]. Its established role as a driver in hepatocellular carcinoma (HCC) led us to select the widely used HCC-derived HepG2 cell line for functional studies. This model provides a pathophysiologically relevant context in which to link our structural insights to FOXM1's oncogenic activity. To assess how FOXM1 influences proliferation and target gene expression, we transfected HepG2 cells with a plasmid encoding C-terminally Flag-tagged full-length wild-type FOXM1 ($FOXM1_{FL}$-Flag). Cell proliferation assay showed that $FOXM1_{FL}$-Flag overexpression significantly enhanced the proliferation rate of HepG2 cells (Figure 5A). In contrast, cells overexpressing $FOXM1_{FL}$-ΔDBD, a DNA-binding domain deletion mutant, displayed a proliferation rate comparable to that of empty vector-transfected controls. Moreover, overexpression of $FOXM1_{FL}$-mut, which carries point mutations in key DBD residues, also led to a reduced proliferation rate, similar to that observed in $FOXM1_{FL}$-ΔDBD-expressing cells (Figure 5A). Western blot analysis confirmed that $FOXM1_{FL}$-Flag, $FOXM1_{FL}$-ΔDBD, and $FOXM1_{FL}$-mut were expressed at comparable levels (Supplementary Figure S5). Collectively, these results indicated that FOXM1-mediated promo-

tion of cell proliferation depended on its DNA-binding capability.

Quantitative PCR analysis further revealed that $FOXM1_{FL}$-Flag overexpression significantly increased the transcript levels of *Vimentin*, *SMAD3*, *CyclinB1*, and *PLK1* (Figure 5B–F). In contrast, cells overexpressing $FOXM1_{FL}$-ΔDBD showed transcript levels similar to those in empty vector-transfected controls, confirming that FOXM1-driven transcriptional activation strictly requires its DNA-binding domain. Similarly, overexpression of $FOXM1_{FL}$-mut resulted in a reduction in transcript levels of these target genes, paralleling the effects seen with the DNA-binding domain deletion mutant (Figure 5B–F).

Discussion

As a member of the evolutionarily conserved FOX family of transcription factors, FOXM1 serves as a pivotal master regulator of the cell cycle, orchestrating the expression of a vast array of genes essential for both mitotic entry and progression [22,23]. The function of FOXM1 is largely dependent on its conserved winged-helix DNA-binding domain, which mediates the recognition of the classic FKH motif of target genes. Our detailed structural and mutational analysis of the FOXM1 DBD reveals a core recognition mechanism that is both universal and specialized across the FOX family. The high-resolution structure demonstrates that FOXM1 employs the canonical winged-helix fold, where its third helix (α3) acts as the primary molecular stylus, reading the genetic code within the DNA major groove. An essential triad—Asn283, Arg286, and His287—mediates sequence-specific DNA recognition through direct hydrogen bonding within the major groove. Moreover, FOXM1 utilizes its auxiliary regions for non-sequence-specific phosphate backbone interactions, collectively ensuring precise accommodation of the DNA duplex. Moreover, DNA mutagenesis and ITC data together with structural insights reveal how specific molecular contacts at each position collectively determine both the affinity and specificity of FOXM1-DNA interactions. In the broader landscape of FOX family structures, the FOXM1-DNA complex presented here does not define a novel overall binding geometry; rather, it provides a high-resolution confirmation of the conserved winged-helix docking paradigm. The primary advance of our work lies in defining the precise, residue-level interaction network—particularly the essential "Asn-Arg-His" triad and its unique pattern of auxiliary contacts—that underlies FOXM1's specificity. This detailed view enables a meaningful comparison with other FOX subfamilies to elucidate how conserved frameworks are diversified for functional specialization.

The FOX family of transcription factors represents a quintessential example of nature's ability to engineer functional diversity from a conserved structural blueprint [32,49]. In terms of conservatism, at the heart of the recognition mechanism of FOX proteins lies the precise docking of the third α-helix (α3, or the "recognition helix") into the major groove of B-form DNA. Our structural data on FOXM1, in concert with prior work on FOXO1, FOXA2, and FOXK1, reveal that this helix is positioned through a network of conserved,

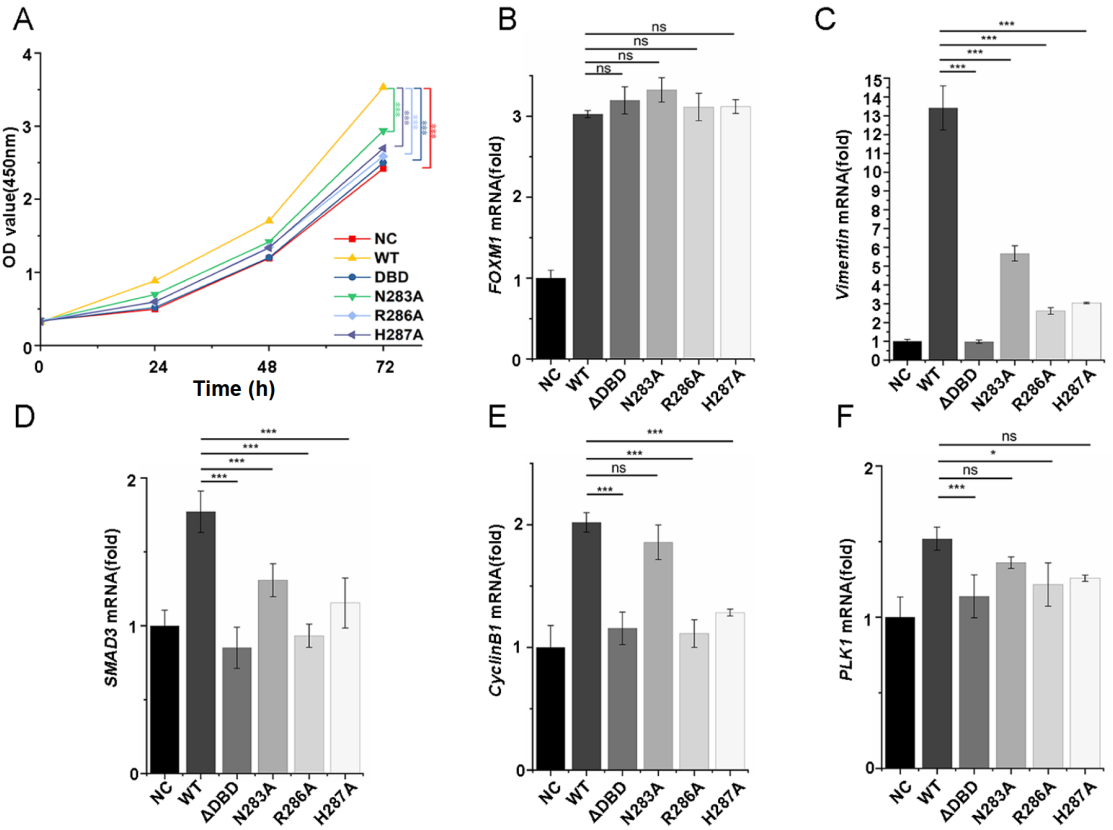


Figure 5. FOXM1 overexpression promotes HepG2 cell proliferation and upregulates the transcription of target genes (A) Effects of wild-type and mutant FOXM1 overexpression on HepG2 cell proliferation, as assessed by CCK-8 assay. (B–F) Quantitative RT-PCR analysis of *FOXM1*, *Vimentin*, *SMAD3*, *Cyclin B1*, and *PLK1* mRNA levels in HepG2 cells transfected with empty vector, $FOXM1_{FL}$-Flag, $FOXM1_{FL}$-ΔDBD, or $FOXM1_{FL}$-mut. Data are presented as the mean ± SD; $n = 3$ biological replicates. Statistical significance was analyzed by one-way ANOVA with Tukey's *post hoc* test; $^*P < 0.05$; ns, not significant.

primarily hydrophobic interactions with the core of the DBD, creating a stable platform from which specific side chains can project into the groove [50–52]. The sequence-specific readout is achieved through a combination of hydrogen bonding and van der Waals contacts by the "Asn-Arg-His" triad. For instance, in FOXM1, the side chain of Asn283 forms a critical bidentate hydrogen bond with an adenine base, an interaction pattern mirrored by Asn211 in FOXO1. Similarly, the ability of His287 in FOXM1 to engage two adjacent thymine bases through a dual hydrogen-bonding network results in its counterpart in His215 of FOXO1. This conservation of specific residue-function relationships underscores a fundamental and optimized "grammar" for reading the RYAAAYA motif, wherein certain amino acids are evolutionarily constrained to recognize specific nucleotides.

Beyond the recognition helix, the so-called "wings" of the DBD play a decisive and highly diversified role in fine-tuning DNA affinity and specificity [53]. W1, typically a short loop following the first β-strand, often mediates critical—albeit largely nonspecific—phosphate backbone contacts, as observed in FOXO1 and FOXA2 structures (Figure 6A,B) [50,51]. However, in FOXM1, W1 contributes fewer interactions with the DNA backbone, which we propose partially accounts for its relatively lower DNA-binding affinity than those of other FOX family DBDs. Moreover, the C-terminal W2 exhibits the most dramatic structural and functional divergence, serving as a key determinant of subfamily identity [54]. In our FOXM1-DBD-dsDNA complex, the W2 region is highly flexible and was not resolved in the electron density map, indicating its lack of direct involvement in DNA recognition. This absence of stabilizing interactions from W2, combined with the limited backbone contacts mediated by W1, likely contributes collectively to the relatively lower DNA-binding affinity of FOXM1 than those of other FOX family members. Striking structural diversity in W2 is evident across the FOX family. In FOXO1, the W2 region is intrinsically disordered and acts as a central hub for post-translational modification, with acetylation of its lysine residues directly modulating DNA affinity through neutralization of positive charges (Figure 6A) [50]. This contrasts sharply with that of FOXK1 and FOXN3, where W2 folds into a stable α-helix that packs against the DNA minor groove, effectively extending the DNA-binding interface (Figure 6C,D) [52,55]. An alternative structural solution is observed in FOXG1, where W2 forms two antiparallel β-strands that engage in phosphate contacts with the DNA backbone (Figure 6E) [56]. This spectrum of W2 architectures—from the flexible and non-participatory conformation in FOXM1 to the disordered yet regulatable form in FOXO1 to the structured, DNA-engaging elements in FOXK1, FOXN3 and FOXG1—illustrates how a single topological module has been evolutionarily tailored to confer distinct biophysical and regulatory properties. Overall, the role of FOXM1 as a master regulator of proliferation is built upon this conserved structural framework but is defined by its unique combination of a rigid, essential α3 triad and flexible wing regions. Furthermore, our mutagenesis data highlight that beyond the sequence-specific α3 helix, non-sequence-specific interactions with the phosphate backbone are critical for stable DNA binding by FOXM1. Mutations in key backbone-contact residues such as Arg236 and Trp308 severely impair affinity, underscoring their role in complex stabilization and precise positioning of the DBD on DNA. This reliance on distributed backbone contacts appears to be a conserved feature across the FOX family for achieving stable docking [57–59]. However, the unique combination of these contacts in FOXM1—coupled with its flexible W2 region, which, unlike the structured or regulatory wings in FOXO1 or FOXK1, provides minimal additional DNA interaction—collectively shapes its distinct DNA-binding interface and may contribute to its

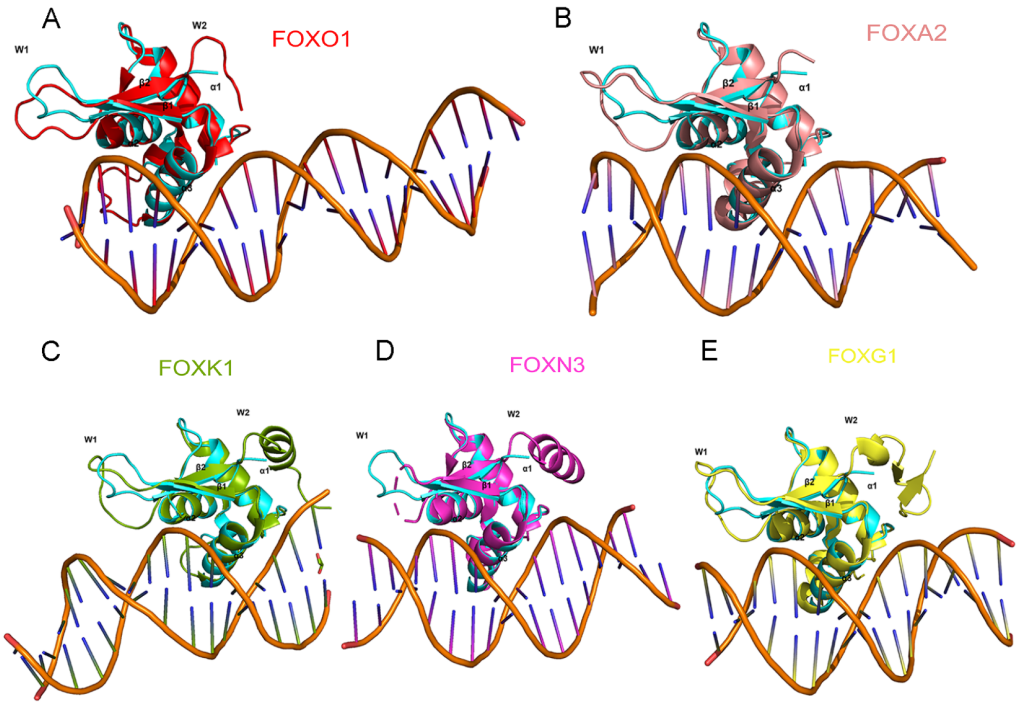


Figure 6. Structural comparison of FOXM1-DBD with other FOX family DNA-binding domains Cartoon representations of FOX protein-DNA complexes superposed with FOXM1-DBD (colored as in Figure 2): (A) FOXO1 (PDB: 5DUI); (B) FOXA2 (PDB: 7YZF); (C) FOXK1 (PDB: 8BZM); (D) FOXN3 (PDB: 6NCE); (E) FOXG1 (PDB: 7CBY).

measured binding affinity relative to other family members. Overall, the role of FOXM1 as a master regulator of proliferation is built upon this conserved structural framework but is defined by its unique combination of a rigid, essential α3 triad and flexible wing regions. This architecture allows FOXM1 to recognize cell cycle gene promoters while remaining responsive to regulatory signals.

Targeting FOXM1 has emerged as a promising anticancer strategy due to its central role in tumor progression and therapy resistance. FOXM1 promotes metastatic dissemination in cancers such as breast and lung cancer through functional interactions with SMAD3 [37]. It also drives resistance to a range of chemotherapeutic agents —including Herceptin and Taxol—by increasing DNA repair capacity, increasing drug efflux, and dysregulating cell cycle progression [60]. Consistent with these findings, FOXM1 inhibition has been shown to sensitize chemoresistant cancer cells to treatments, particularly DNA-damaging agents, highlighting its therapeutic relevance [61].

The well-defined, structured nature of the FOXM1-DNA interface, centered on its essential α3-helix triad, offers a highly promising target for therapeutic intervention. Disruption of this interface could selectively block FOXM1's oncogenic transcriptional program, providing a novel alternative to conventional kinase inhibitors. Although the complete molecular network through which FOXM1 regulates tumor growth and metastasis remains incompletely understood, further elucidation of these mechanisms will be essential for developing subtype-specific therapies, identifying predictive biomarkers, and ultimately improving clinical outcomes.

Supplementary Data

Supplementary data are available at *Acta Biochimica et Biophysica Sinica* online.

Data Availability

The atomic coordinates and structure factors (PDB ID: 9XS1) have been deposited in the Protein Data Bank (http://www.pdb.org/). All other data can be accessed upon reasonable request from the corresponding authors.

Acknowledgement

We would like to thank the staff at the BL19U1 and BL02U1 beamlines at the SSRF (Shanghai, China) for providing technical support in X-ray diffraction data collection and analysis.

Funding

This work was supported by the grants from the National Natural Science Foundation of China (No. 32293213 to Y.S. and M.L.; No. 32100958 to M.L.; Nos. 32293210, 32149302 and 32090040 to Y.S.), and the Strategic Priority Research Program of the Chinese Academy of Sciences (Nos. XDB39010300 and XDB37010105 to Y.S.).

Conflict of Interest

The authors declare that they have no conflict of interest.

References

1. Huber K, Mestres-Arenas A, Fajas L, Leal-Esteban LC. The multifaceted role of cell cycle regulators in the coordination of growth and metabolism. *FEBS J* 2021, 288: 3813–3833
2. Wiman KG, Zhivotovsky B. Understanding cell cycle and cell death regulation provides novel weapons against human diseases. *J Intern Med* 2017, 281: 483–495
3. Matthews HK, Bertoli C, de Bruin RAM. Cell cycle control in cancer. *Nat Rev Mol Cell Biol* 2022, 23: 74–88
4. Bu H, Pei C, Ouyang M, Chen Y, Yu L, Huang X, Tan Y. The antitumor peptide M1-20 induced the degradation of CDK1 through CUL4-DDB1-DCAF1-involved ubiquitination. *Cancer Gene Ther* 2025, 32: 61–70
5. Davies M, Boyce M, Conway E. Short circuit: transcription factor addiction as a growing vulnerability in cancer. *Curr Opin Struct Biol* 2024, 89: 102948
6. Chen A, Koehler AN. Transcription factor inhibition: lessons learned and emerging targets. *Trends Mol Med* 2020, 26: 508–518
7. de Jonge WJ, Patel HP, Meeussen JVW, Lenstra TL. Following the tracks: how transcription factor binding dynamics control transcription. *Biophys J* 2022, 121: 1583–1592
8. Shiah JV, Johnson DE, Grandis JR. Transcription factors and cancer. *Cancer J* 2023, 29: 38–46
9. Cheng C, Li LM. Systematic identification of cell cycle regulated transcription factors from microarray time series data. *BMC Genomics* 2008, 9: 116
10. Kovacs LAS, Orlando DA, Haase SB. Transcription network and cyclin/CDKs: the yin and yang of cell cycle oscillators. *Cell Cycle* 2008, 7: 2626–2629
11. Bu H, Lan X, Cheng H, Pei C, Ouyang M, Chen Y, Huang X, *et al.* Development of an interfering peptide M1-20 with potent anti-cancer effects by targeting FOXM1. *Cell Death Dis* 2023, 14: 533
12. Vishnoi K, Viswakarma N, Rana A, Rana B. Transcription factors in cancer development and therapy. *Cancers* 2020, 12: 2296
13. Pacini C, Duncan E, Gonçalves E, Gilbert J, Bhosle S, Horswell S, Karakoc E, *et al.* A comprehensive clinically informed map of dependencies in cancer cells and framework for target prioritization. *Cancer Cell* 2024, 42: 301–316.e9
14. Xue L, Chiang L, He B, Zhao YY, Winoto A, Unutmaz D. FoxM1, a forkhead transcription factor is a master cell cycle regulator for mouse mature T cells but not double positive thymocytes. *PLoS One* 2010, 5: e9229
15. Zhang Z, Li M, Sun T, Zhang Z, Liu C. FOXM1: functional roles of FOXM1 in non-malignant diseases. *Biomolecules* 2023, 13: 857
16. Chen T, Ni M, Wang H, Xue F, Jiang T, Wu X, Li C, *et al.* The reparative effect of FOXM1 in pulmonary disease. *Lung* 2025, 203: 1
17. Khan MA, Khan P, Ahmad A, Fatima M, Nasser MW. FOXM1: A small fox that makes more tracks for cancer progression and metastasis. *Semin Cancer Biol* 2023, 92: 1–15
18. Yang C, Chen H, Tan G, Gao W, Cheng L, Jiang X, Yu L, *et al.* FOXM1 promotes the epithelial to mesenchymal transition by stimulating the transcription of Slug in human breast cancer. *Cancer Lett* 2013, 340: 104–112
19. Zhang YL, Ma Y, Zeng YQ, Liu Y, He EP, Liu YT, Qiao FL, *et al.* A narrative review of research progress on FoxM1 in breast cancer carcinogenesis and therapeutics. *Ann Transl Med* 2021, 9: 1704
20. Jackson BC, Carpenter C, Nebert DW, Vasiliou V. Update of human and mouse forkhead box (FOX) gene families. *Hum Genomics* 2010, 4: 345
21. Laoukili J, Stahl M, Medema RH. FoxM1: at the crossroads of ageing and cancer. *Biochim Biophys Acta Rev Cancer* 2007, 1775: 92–102
22. He F, Liu H, Zhao F. The oncogenic role of FOXM1 in hepatocellular carcinoma: molecular mechanisms, clinical significance, and therapeutic potentials. *Naunyn Schmiedebergs Arch Pharmacol* 2025, 398: 13121–13152
23. Kalathil D, John S, Nair AS. FOXM1 and cancer: faulty cellular signaling

derails homeostasis. *Front Oncol* 2021, 10: 626836
24. Jiang X, Liu J, Wang K, Sun J, Yin H, Jiang Y, Liu Y, ***et al.*** ASPM mediates nuclear entrapment of FOXM1 via liquid-liquid phase separation to promote progression of hepatocarcinoma. *Genome Biol* 2025, 26: 68
25. Liao GB, Li XZ, Zeng S, Liu C, Yang SM, Yang L, Hu CJ, ***et al.*** Regulation of the master regulator FOXM1 in cancer. *Cell Commun Signal* 2018, 16: 57
26. Katzenellenbogen BS, Guillen VS, Katzenellenbogen JA. Targeting the oncogenic transcription factor FOXM1 to improve outcomes in all subtypes of breast cancer. *Breast Cancer Res* 2023, 25: 76
27. Zhang Y, Ding N, Li Y, Ouyang M, Fu P, Peng Y, Tan Y. Transcription factor FOXM1 specifies chromatin DNA to extracellular vesicles. *Autophagy* 2024, 20: 1054–1071
28. Marceau AH, Brison CM, Nerli S, Arsenault HE, McShan AC, Chen E, Lee HW, ***et al.*** An order-to-disorder structural switch activates the FoxM1 transcription factor. *eLife* 2019, 8: e46131
29. Engeland K. Cell cycle regulation: P53-p21-RB signaling. *Cell Death Differ* 2022, 29: 946–960
30. Weiler SME, Pinna F, Wolf T, Lutz T, Geldiyev A, Sticht C, Knaub M, ***et al.*** Induction of chromosome instability by activation of Yes-associated protein and forkhead box M1 in liver cancer. *Gastroenterology* 2017, 152: 2037–2051.e22
31. Park HJ, Costa RH, Lau LF, Tyner AL, Raychaudhuri P. Anaphase-promoting complex/cyclosome-Cdh1-mediated proteolysis of the forkhead box m1 transcription factor is critical for regulated entry into s phase. *Mol Cell Biol* 2008, 28: 5162–5171
32. Golson ML, Kaestner KH. Fox transcription factors: from development to disease. *Development* 2016, 143: 4558–4570
33. Xie F, Zhou X, Ran Y, Li R, Zou J, Wan S, Su P, ***et al.*** Targeting FOXM1 condensates reduces breast tumour growth and metastasis. *Nature* 2025, 638: 1112–1121
34. Wang IC, Chen YJ, Hughes D, Petrovic V, Major ML, Park HJ, Tan Y, ***et al.*** Forkhead box M1 regulates the transcriptional network of genes essential for mitotic progression and genes encoding the SCF (Skp2-Cks1) ubiquitin ligase. *Mol Cell Biol* 2005, 25: 10875–10894
35. Zhang J, Zhang J, Cui X, Yang Y, Li M, Qu J, Li J, ***et al.*** FoxM1: a novel tumor biomarker of lung cancer. *Int J Clin Exp Med* 2015, 8: 3136–3140
36. Cheng H, Yuan J, Pei C, Ouyang M, Bu H, Chen Y, Huang X, ***et al.*** The development of an anti-cancer peptide M1-21 targeting transcription factor FOXM1. *Cell Biosci* 2023, 13: 114
37. Zhang Z, Bu H, Yu J, Chen Y, Pei C, Yu L, Huang X, ***et al.*** The cell-penetrating FOXM1 N-terminus (M1-138) demonstrates potent inhibitory effects on cancer cells by targeting FOXM1 and FOXM1-interacting factor SMAD3. *Theranostics* 2019, 9: 2882–2896
38. Lv M, Gao J, Li M, Ma R, Li F, Liu Y, Liu M, ***et al.*** Conformational selection in ligand recognition by the first tudor domain of PHF20L1. *J Phys Chem Lett* 2020, 11: 7932–7938
39. Vagin A, Teplyakov A. Molecular replacement with MOLREP. *Acta Crystlogr D Biol Crystlogr* 2010, 66: 22–25
40. Emsley P, Lohkamp B, Scott WG, Cowtan K. Features and development of Coot. *Acta Crystlogr D Biol Crystlogr* 2010, 66: 486–501
41. Murshudov GN, Vagin AA, Dodson EJ. Refinement of macromolecular structures by the maximum-likelihood method. *Acta Crystlogr D Biol Crystlogr* 1997, 53: 240–255
42. Murshudov GN, Skubák P, Lebedev AA, Pannu NS, Steiner RA, Nicholls RA, Winn MD, ***et al.*** REFMAC5 for the refinement of macromolecular crystal structures. *Acta Crystlogr D Biol Crystlogr* 2011, 67: 355–367
43. Adams PD, Afonine PV, Bunkóczi G, Chen VB, Davis IW, Echols N, Headd JJ, ***et al.*** PHENIX: a comprehensive Python-based system for macro-molecular structure solution. *Acta Crystlogr D Biol Crystlogr* 2010, 66: 213–221
44. Xiang Q, Tan G, Jiang X, Wu K, Tan W, Tan Y. Suppression of FOXM1 transcriptional activities via a single-stranded DNA aptamer generated by SELEX. *Sci Rep* 2017, 7: 45377
45. Iness AN, Litovchick L. MuvB: a key to cell cycle control in ovarian cancer. *Front Oncol* 2018, 8: 223
46. Shin SB, Jang HR, Xu R, Won JY, Yim H. Active PLK1-driven metastasis is amplified by TGF-β signaling that forms a positive feedback loop in non-small cell lung cancer. *Oncogene* 2020, 39: 767–785
47. Jang HR, Shin SB, Kim CH, Won JY, Xu R, Kim DE, Yim H. PLK1/vimentin signaling facilitates immune escape by recruiting Smad2/3 to PD-L1 promoter in metastatic lung adenocarcinoma. *Cell Death Differ* 2021, 28: 2745–2764
48. Tan Y, Chen Y, Yu L, Zhu H, Meng X, Huang X, Meng L, ***et al.*** Two-fold elevation of expression of FoxM1 transcription factor in mouse embryonic fibroblasts enhances cell cycle checkpoint activity by stimulating *p21* and *Chk1* transcription. *Cell Prolif* 2010, 43: 494–504
49. Hannenhalli S, Kaestner KH. The evolution of Fox genes and their role in development and disease. *Nat Rev Genet* 2009, 10: 233–240
50. Singh P, Han EH, Endrizzi JA, O'Brien RM, Chi YI. Crystal structures reveal a new and novel FoxO1 binding site within the human glucose-6-phosphatase catalytic subunit 1 gene promoter. *J Struct Biol* 2017, 198: 54–64
51. Pluta R, Aragón E, Prescott NA, Ruiz L, Mees RA, Baginski B, Flood JR, ***et al.*** Molecular basis for DNA recognition by the maternal pioneer transcription factor FoxH1. *Nat Commun* 2022, 13: 7279
52. Xie Z, Sokolov I, Osmala M, Yue X, Bower G, Pett JP, Chen Y, ***et al.*** DNA-guided transcription factor interactions extend human gene regulatory code. *Nature* 2025, 641: 1329–1338
53. Marsden I, Chen Y, Jin C, Liao X. Evidence that the DNA binding specificity of winged helix proteins is mediated by a structural change in the amino acid sequence adjacent to the principal DNA binding helix. *Biochemistry* 1997, 36: 13248–13255
54. Littler DR, Alvarez-Fernandez M, Stein A, Hibbert RG, Heidebrecht T, Aloy P, Medema RH, ***et al.*** Structure of the FoxM1 DNA-recognition domain bound to a promoter sequence. *Nucleic Acids Res* 2010, 38: 4527–4538
55. Rogers JM, Waters CT, Seegar TCM, Jarrett SM, Hallworth AN, Blacklow SC, Bulyk ML. Bispecific forkhead transcription factor foxn3 recognizes two distinct motifs with different DNA shapes. *Mol Cell* 2019, 74: 245–253.e6
56. Dai S, Li J, Zhang H, Chen X, Guo M, Chen Z, Chen Y. Structural basis for DNA recognition by FOXG1 and the characterization of disease-causing FOXG1 mutations. *J Mol Biol* 2020, 432: 6146–6156
57. Zhang H, Dai S, Liang X, Li J, Chen Y. Mechanistic insights into the preference for tandem binding sites in DNA recognition by FOXM1. *J Mol Biol* 2022, 434: 167426
58. Stroud JC, Wu Y, Bates DL, Han A, Nowick K, Paabo S, Tong H, ***et al.*** Structure of the forkhead domain of FOXP2 bound to DNA. *Structure* 2006, 14: 159–166
59. Dai S, Qu L, Li J, Chen Y. Toward a mechanistic understanding of DNA binding by forkhead transcription factors and its perturbation by pathogenic mutations. *Nucleic Acids Res* 2021, 49: 10235–10249
60. Carr JR, Park HJ, Wang Z, Kiefer MM, Raychaudhuri P. FoxM1 mediates resistance to herceptin and paclitaxel. *Cancer Res* 2010, 70: 5054–5063
61. Raghuwanshi S, Gartel AL. Small-molecule inhibitors targeting FOXM1: current challenges and future perspectives in cancer treatments. *Biochim Biophys Acta Rev Cancer* 2023, 1878: 189015